AGU PUBLICATIONS

JGR

Journal of Geophysical Research: Space Physics

BRIEF REPORT

10.1002/2014JA020028

Key Points:
- The observed equatorward winds around the cusp have been reproduced by GITM
- The impact of cusp energy on the horizontal neutral winds has been studied
- The influence of resolution on cusp simulation has also been investigated

Supporting Information:
- Figure S1

Correspondence to:
C. Sheng,
cheng.sheng@mavs.uta.edu

Citation:
Sheng, C., Y. Deng, Q. Wu, A. Ridley, and I. Häggström (2015), Thermospheric winds around the cusp region, *J. Geophys. Res. Space Physics*, *120*, 1248–1255, doi:10.1002/2014JA020028.

Received 31 MAR 2014
Accepted 30 DEC 2014
Accepted article online 7 JAN 2015
Published online 3 FEB 2015

Thermospheric winds around the cusp region

Cheng Sheng[1], Yue Deng[1], Qian Wu[2], Aaron Ridley[3], and Ingemar Häggström[4]

[1]Department of Physics, University of Texas at Arlington, Arlington, Texas, USA, [2]High Altitude Observatory, National Center for Atmospheric Research, Boulder, Colorado, USA, [3]Department of Atmospheric, Oceanic and Space Sciences, University of Michigan, Ann Arbor, Michigan, USA, [4]EISCAT, Kiruna, Sweden

Abstract An equatorward wind has been observed first by the balloon-borne Fabry-Perot interferometer called High-Altitude Interferometer Wind Observation on the equatorward side of the cusp near the local noon, which is opposite to the typical direction of neutral wind driven by the day-night pressure gradient. However, this dayside equatorward wind was not reproduced by the standard Thermosphere Ionosphere Electrodynamics General Circulation Model under the resolution of 5° longitude by 5° latitude (5° × 5°). In this study, the Global Ionosphere Thermosphere Model has been run in different cases and under different resolutions to investigate the neutral dynamics around the cusp region. First, we compare the simulations with and without additional cusp energy inputs to identify the influence of cusp heating. Both runs have a resolution of 5° × 1° (longitude × latitude) in order to better resolve the cusp region. After adding in the cusp energy, the meridional wind in simulation turns to be equatorward on the dayside, which is consistent with the observation. It indicates that strong heating in the cusp region causes changes in the pressure gradient around the cusp and subsequent variations in the neutral winds. The simulations with the same cusp heating specifications are repeated, but with different horizontal resolutions to examine the influence of resolution on the simulation results. The comparisons show that the resolution of 5° × 1° can resolve the cusp region much more stably and consistently than the 5° × 5° resolution.

1. Introduction

The horizontal thermospheric winds are mainly driven by the pressure gradient, the Coriolis force, the ion drag, and viscosity [*Rishbeth*, 1972], which are strongly controlled by solar irradiance and other energy sources, such as auroral heating and gravity waves [*Killeen et al.*, 1995; *Titheridge*, 1995; *Rees et al.*, 1984]. The dynamics of thermosphere still represents the biggest challenge for both observations and simulations in the community, although it has been studied extensively [*Killeen and Roble*, 1988; *Thayer et al.*, 1995; *Deng and Ridley*, 2006; *Meriwether*, 2006]. In the cusp region, one would normally expect an antisunward flow, since the gradient in pressure and ion drag forces are often in the same direction. However, in *Wu et al.* [2012], a persistent equatorward wind has been observed on the dayside near the cusp region using the balloon-borne Fabry-Perot interferometer called HIWIND (High-Altitude Interferometer Wind Observation). Meanwhile, the observed equatorward wind was not reproduced by the standard Thermosphere Ionosphere Electrodynamics General Circulation Model (TIEGCM) under the resolution of 5° × 5° in longitude and latitude [*Wu et al.*, 2012]. The equatorward wind is opposite to the direction of neutral wind driven by the day-night pressure gradient, which requires an additional force or energy to reverse the direction of meridional wind. Since the HIWIND balloon was able to observe on the equatorward side of the cusp during daytime, the cusp energy may be a potential driver for the equatorward meridional wind.

The cusp and its effect on the ionosphere and thermosphere have been of great interest because of its unique characteristics in the way to couple to the solar wind through energy, momentum, and mass [*Eather*, 1985; *Smith and Lockwood*, 1996]. Using conjugate observations from European Incoherent Scatter (EISCAT) radar, Magnetometers-Ionospheric Radars-All-Sky Cameras Large Experiment, and Cluster, *Yordanova et al.* [2007] showed that the energy including the Poynting flux and particle precipitation (with the characteristic energy of tens to several hundred eV) from the exterior cusp (~9 *Re*) contributed to the heating in the ionosphere below. The Poynting flux to the ionosphere can be estimated from the electric field and perturbed magnetic field, by applying the Poynting flux theorem [*Kelley et al.*, 1991; *Richmond*, 2010]. The measurements from the Defense Meteorological Satellite Program (DMSP) F-15 satellite showed that in an extreme case the Poynting flux exceeded 100 mW/m^2 in and near the cusp region [*Knipp et al.*, 2011]. Additionally, a significant amount of particles precipitate in the cusp with typical energies of 100–200 eV

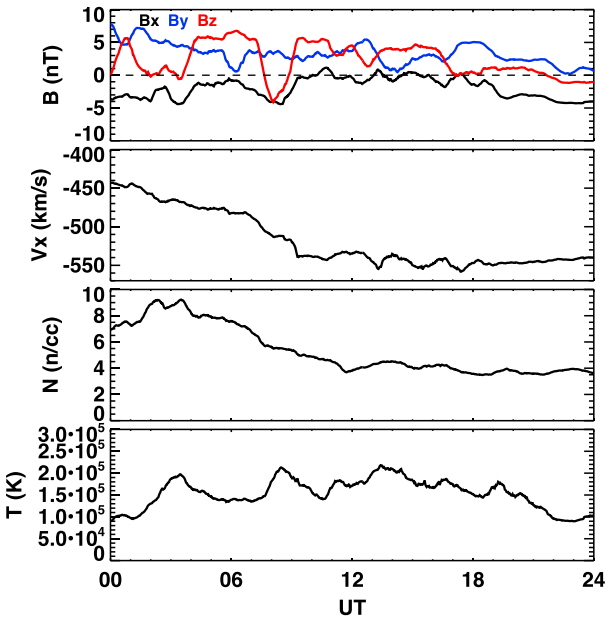

Figure 1. Solar wind and IMF conditions on 14 June 2011. (from top to bottom) IMF B_X, B_Y, and B_Z, solar wind speed V_X, proton density, and proton temperature.

(electrons) and 1–2 keV (ions) [*Frey*, 2007]. To explain the neutral density enhancements observed by the Challenging Minisatellite Payload (CHAMP) satellite [*Lühr et al.*, 2004; *Rentz and Lühr*, 2008], *Deng et al.* [2013] carried out a theoretical study using the Global Ionosphere Thermosphere Model (GITM) [*Ridley et al.*, 2006], in which the influence of Poynting flux and particle precipitation on the cusp region was investigated. The total effect of a Poynting flux of 75 mW/m^2 and 100 eV, 2 mW/m^2 soft electron precipitation results in a neutral density enhancement at 400 km by more than 50%, which is consistent with the CHAMP observations in extreme cases.

In this paper, the impact of cusp energy on the horizontal wind near the cusp location has been assessed by using GITM. The simulations have been compared with HIWIND neutral wind observation. GITM is run with a resolution of 5° longitude by 1° latitude to better resolve the small cusp region. Two different cases (with and without additional cusp energy) have been compared to identify the influence of cusp energy on the neutral dynamics. GITM simulations under different resolutions have also been studied to analyze the difficulty for general circulation models (GCMs) to simulate the cusp region.

2. Methodology

The Global Ionosphere Thermosphere Model (GITM) is a three-dimensional, self-consistent general circulation model [*Ridley et al.*, 2006], which solves for the neutral and ion densities, velocities and temperatures. The most significant differences between GITM and other GCMs are the flexible resolution and the nonhydrostatic feature. In GITM the number of grid points in each direction can be specified at runtime, which makes the resolution in GITM quite flexible. Meanwhile, GITM does not assume a hydrostatic equilibrium in the vertical direction. The hydrostatic equilibrium has been assumed in most GCMs, and the assumption is valid in large-scale phenomena when the vertical pressure gradient force is roughly balanced with the gravitational force. However, the atmosphere can be out of hydrostatic equilibrium, or the vertical pressure gradient force and gravitational force are out of balance, when there are substantial energy inputs at some localized region such as cusp. Therefore, the nonhydrostatic model with high resolution does have some advantage to simulate the cusp region. In this study, GITM has been run with resolutions of 5° × 1° in longitude and latitude and 5° × 5°.

The simulations last for 48 h from 0000 UT 13 June to 2400 UT 14 June 2011. Indices, including $F_{10.7}$ index, solar wind and interplanetary magnetic field (IMF) conditions, and NOAA hemispheric power, are used to drive the model. Solar wind and IMF conditions on 14 June s2011 have been plotted out in Figure 1 for reference. One minute resolution OMNI data is used and is smoothed with an averaging window of 45 min. During most of the time, IMF B_Z is between −5 nT and 8 nT, and the magnitude of IMF B_Y is smaller than 10 nT in general. These IMF conditions indicate a quiet or a moderate geomagnetic storm period. The *Weimer* [1996] empirical model is used to specify the electrodynamic potential patterns at high latitudes, and the *Fuller-Rowell and Evans* [1987] empirical model is used for the auroral particle precipitation in GITM. The model is run for 24 h first to reach a quasi steady state. Then two cases, without and with additional cusp energy are simulated, and the difference between them represents the influence of additional cusp energy. The additional cusp energy includes Poynting flux and soft particle precipitation. Soft proton precipitation (with characteristic energy of several keV) is not considered here, since the protons mostly

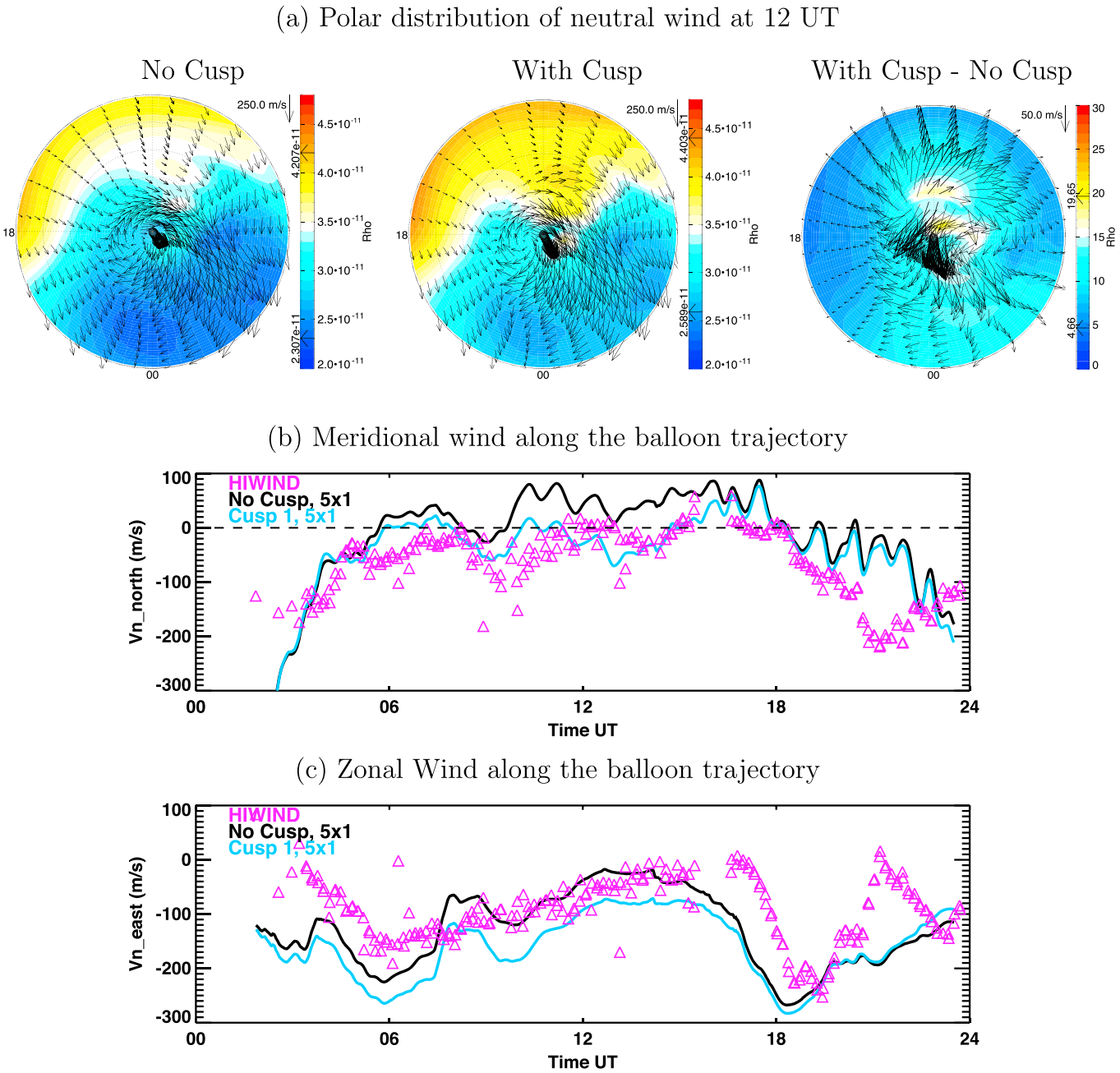

Figure 2. (a) GITM simulations of neutral density (color contour, in the unit of kg/m^3) and horizontal neutral wind (vector) at 12 UT on 14 June 2011 and 250 km altitude (left) without and (middle) with additional cusp energy. (right) Their difference (with cusp - no cusp) is shown, in which the color contour is the percentage difference in neutral density. The outer boundary is 40°N. Comparisons of (b) meridional and (c) zonal winds between simulations and observation along the balloon trajectory on 14 June 2011. The magenta triangle is for HIWIND observation, the black line is for GITM simulation without additional cusp energy, and the blue line is for GITM simulation with the additional cusp energy.

penetrate into *E* region altitudes and have little effect at higher altitudes [*Vontrat-Reberac et al.*, 2001; *Deng et al.*, 2013]. Based on previous studies [*Newell and Meng*, 1992; *Zhou et al.*, 2000; *Frey*, 2007; *Knipp et al.*, 2011], the cusp region is set to be 3° in latitude and 6 h in local time, centered at 73.5°N and 1200 LT. A Poynting flux of 20 mW/m^2 and soft electron precipitation of 150 eV, 1 mW/m^2 are imposed in the cusp, representing the cusp region under moderate conditions. The additional Poynting flux is converted to Joule heating and distributed proportionally to the Pedersen conductivity in altitude. The ionization rate of soft electron precipitation is determined based on the parameterization given by *Fang et al.* [2008].

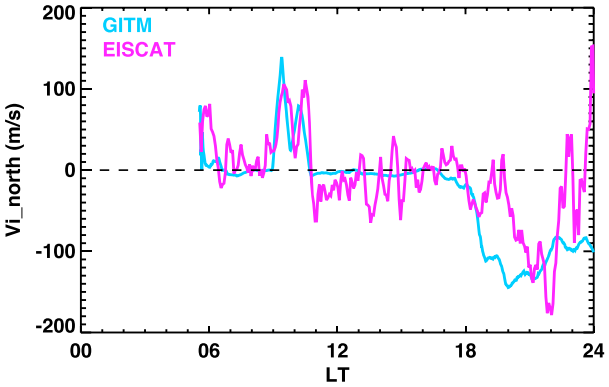

Figure 3. Comparison of meridional ion drift between GITM simulation and EISCAT observation over Kiruna (68°N, 20°E). EISCAT observation is in magenta, and GITM simulation is in blue.

Usually, the momentum and energy are coupled to each other. When additional energy has been added in, the momentum should be changed correspondingly. However, the energy input in the cusp is primarily caused by the electric field variability instead of the average electric field. Its net effect on the momentum should be relatively small after one oscillation cycle since the flip back and forth will not contribute too much to the momentum on average. Therefore, the influence on the momentum in the cusp has not been included in this study.

3. Results and Discussion

3.1. GITM Simulations: With Versus Without Additional Cusp Energy

Figure 2a shows the simulation results at 1200 UT on 14 June 2011 at 250 km altitude under the resolution of 5° longitude by 1° latitude. The left polar distribution, with the outer boundary of 40°N, shows the simulation without additional cusp energy. The color contour is the neutral density, and the vector shows the horizontal neutral wind. Driven by the day-night pressure gradient, the meridional wind at the equatorward of the cusp region is poleward, which is similar to the TIEGCM simulation [*Wu et al.*, 2012]. Figure 2a (middle) shows the simulation with the additional cusp energy. An enhancement in the neutral density appears around the cusp region, which arises from the thermal expansion and corresponding upward vertical wind [*Deng et al.*, 2013]. Meanwhile, the neutral wind on the equatorward side of the cusp region turned equatorward. Figure 2a (right) shows the difference between the simulations with and without additional cusp energy. The color contour shows the percentage difference in neutral density, and the vector shows the difference in the horizontal neutral wind. The enhancement of neutral density is 15% around the cusp region, which is much smaller than the value (50%) in *Deng et al.* [2013]. This is reasonable since the cusp energy in *Deng et al.* [2013] is almost 3 times larger than that used in this study. Additionally, the reported altitudes are different. The vector shows that the neutral wind difference field has a strong divergence around the cusp, which is equatorward on the dayside of cusp and poleward on the nightside.

Figures 2b and 2c show the comparisons of meridional and zonal winds between simulations and HIWIND observation along the balloon trajectory on 14 June 2011. HIWIND observation is in magenta, simulation without additional cusp energy is in black, and simulation with the additional cusp energy is in blue. Without additional cusp energy, the GITM simulation shows poleward meridional wind (positive in Figure 2b) on the dayside (between 0600 LT and 1800 LT), which is similar to the TIEGCM results obtained by *Wu et al.* [2012]. But with the additional cusp energy, the meridional wind on the dayside turns equatorward (negative in Figure 2b), which is consistent with the HIWIND observation. As shown in Figure 2c, the additional cusp energy also causes differences in the zonal wind, since it changes the pressure gradient in the zonal direction as well. However, the inaccuracy in the polar electrodynamics specification from the empirical model [*Weimer*, 1996] may bring in some uncertainties in the zonal wind and cause differences between simulation and observation. The difference between the cases with and without additional cusp energy strongly indicates that the geomagnetic energy in the cusp is one of the drivers for the dayside equatorward neutral wind.

Ion drag and pressure gradient forces often dominate for *F* region winds at high latitudes [*Rishbeth*, 1972], which suggests that the ion drag force should also be taken into account when analyzing the neutral wind variation around the cusp region. Comparison of meridional ion drift between GITM simulation and EISCAT observation over Kiruna (68°N, 20°E), where HIWIND was launched, on 14 June 2011 is shown in Figure 3. They are in agreement on large-scale variation, while some details including the magnitude and turning point are slightly different. Therefore, the *Weimer* [1996] empirical model gives a reasonable

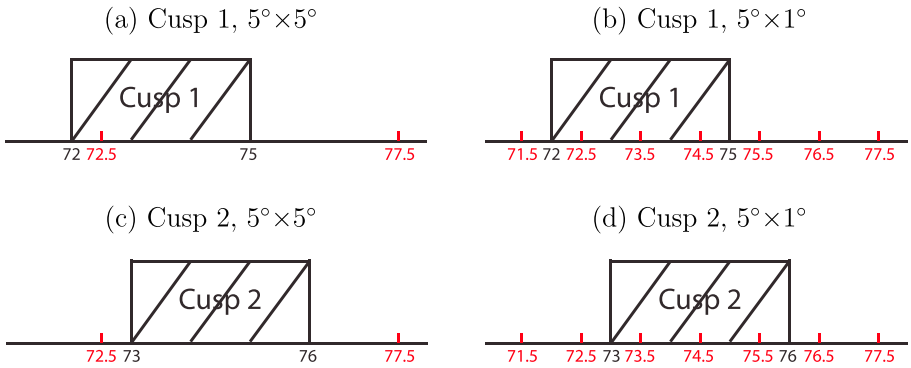

Figure 4. Location of the cusp region (black box) and latitudinal simulation grid point (red point) for different resolutions and cusp configurations. (a and b) The situation when the cusp is located at 72°–75° latitude (Cusp 1) and (c and d) the situation when the cusp is located at 73°–76° latitude (Cusp 2). Figures 4a and 4c show the cases with the resolution of 5° longitude by 5° latitude (5° × 5°), and Figures 4b and 4d show the cases with the resolution of 5° × 1°.

representation of the climatological high-latitude convection pattern. Precisely specifying the high-latitude forcing including both ion drift and energy is a well-known challenge for the community, and certainly improvement is needed for future studies. In this study, we focus on the cusp energy impact on the neutral dynamics.

3.2. Influence of Simulation Resolution

Accurately simulating the cusp is very challenging for most GCMs, since the size of the cusp is often small and its location is often quite variable [*Newell and Meng*, 1987; *Newell et al.*, 1989; *Zhou et al.*, 2000]. This means that GCMs with larger grid/cell sizes may have a difficult time simulating the reaction to the cusp than GCMs with higher resolutions. In this study, two situations under two different resolutions are investigated. Figure 4 shows the location of the cusp (black box) and latitudinal simulation grid point (red point). For the first situation (Cusp 1), the cusp is located from 72° to 75° as shown in Figures 4a and 4b. For the second situation (Cusp 2), the cusp is located from 73° to 76° as shown in Figures 4c and 4d, which is shifted poleward by 1∘ compared with Cusp 1. The two resolutions are 5° × 5° in longitude and latitude (Figures 4a and 4c) and 5° × 1° (Figures 4b and 4d). Under the resolution of 5° × 5°, there is one simulation grid point located inside Cusp 1, but there is no simulation grid point located inside Cusp 2. However, under the resolution of 5° × 1°, there are always three grid points inside the cusp region (both Cusp 1 and Cusp 2), which means the resolution of 5° × 1° can always resolve the small cusp region. Conversely, the 5° × 5° resolution cannot resolve the cusp region some of the time. The cusp is a subgrid process and may fall into the gap between grid points.

Figure 5a shows the difference between the simulations with Cusp 1 and without additional cusp energy at 1200 UT at 250 km altitude under the resolution of 5° × 5°. The color contour shows the percentage difference in neutral density, and the vector shows the difference in horizontal wind. Since one latitudinal grid point is inside the cusp region, the influence of additional cusp energy is represented in the simulation, including an enhancement in the neutral density and a clear difference in the meridional wind around the cusp region. Figure 5c shows the difference between the simulations with Cusp 2 and without additional cusp energy under the resolution of 5° × 5°. No difference is revealed from the figure as expected, since the cusp falls completely between grid points and is not resolved in this particular case.

Figures 5b and 5d are the same as Figures 5a and 5c, but under the resolution of 5° × 1°. Both of them show the neutral density enhancement around the cusp region at 250 km altitude and the significant difference in the neutral wind around the cusp region. The difference between Figure 5b and Figure 5d is quite small, since the specification of cusp location between Cusp 1 and Cusp 2 is very close. The similarity between the simulations with Cusp 1 and with Cusp 2 indicates that using a resolution of 5° × 1° can give a more stable and reliable representation of the cusp than using a resolution of 5° × 5°.

The neutral density enhancement around the cusp region is 38% in Figure 5a and 20% in Figure 5b. The simulations are both with Cusp 1 but are conducted under different resolutions. The magnitude difference of the neutral density enhancement is related to the total energy input into the cusp. With the same energy

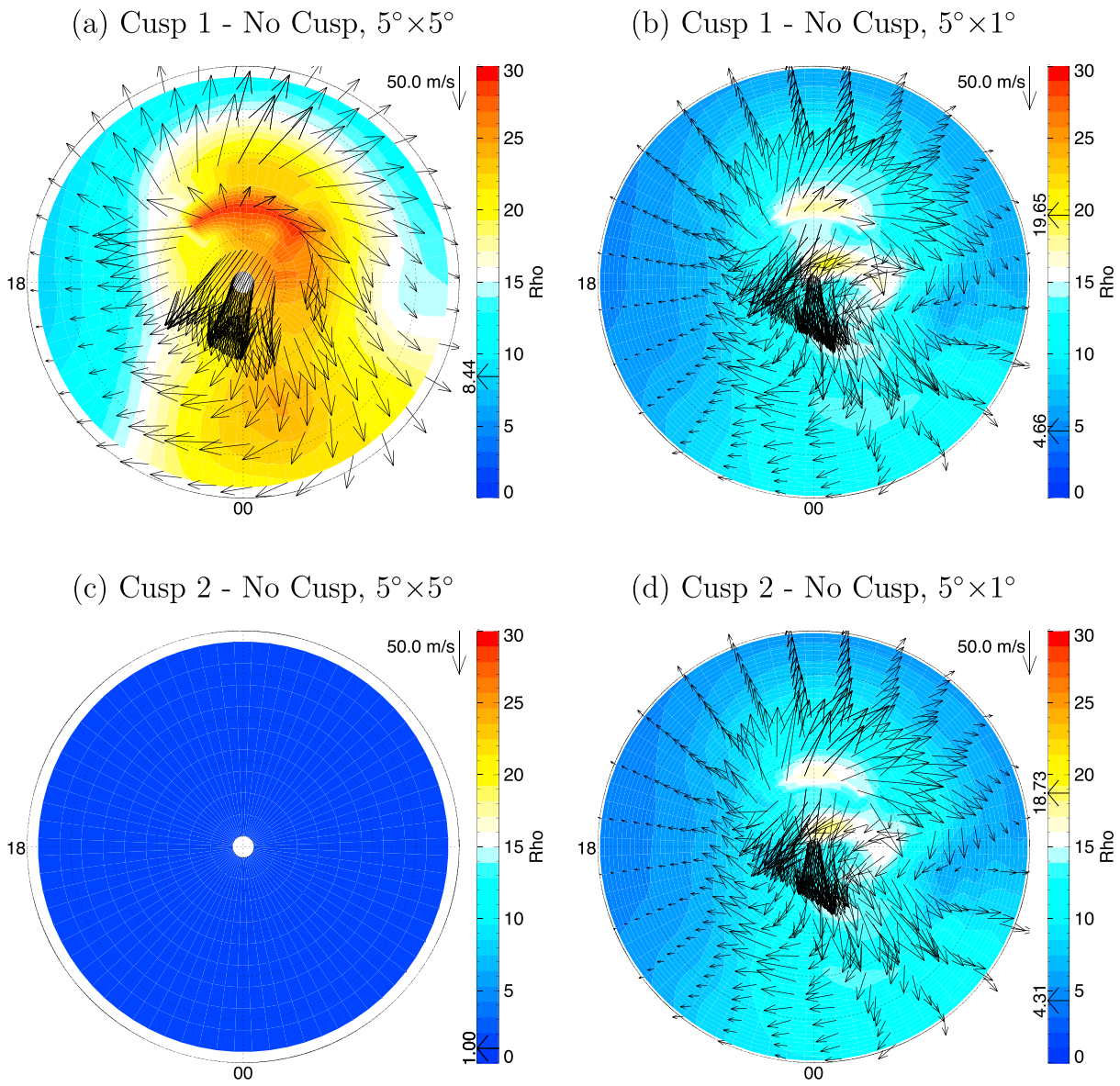

Figure 5. Difference at 12 UT on 14 June 2011 and 250 km altitude between the simulations with and without additional cusp energy under different resolutions. The color contour represents the percentage difference in neutral density, and the vector shows the horizontal wind difference. (a) Difference between simulations with Cusp 1 and without additional cusp energy under the resolution of 5° × 5°. (b) The same as Figure 5a, but under the resolution of 5° × 1°. (c) Difference between simulations with Cusp 2 and without additional cusp energy under the resolution of 5°×5°. (d) The same as Figure 5c, but under the resolution of 5°×1°.

flux, more energy is deposited in the cusp under the resolution of 5° × 5°. In 5° × 5°, the grid size is 5∘ in latitude and larger than the real size of the cusp; therefore, the cusp energy flux is added over a window of 5∘ in latitude. But under the resolution of 5°×1°, the grid size is 1∘ in latitude and smaller than the size of the cusp. The energy is deposited in a window of 3∘ in latitude. Since the local time coverage is the same, the area with cusp energy under the resolution of 5° × 5° is larger than that under the resolution of 5° × 1°. Thus, the total energy in the entire cusp region becomes larger, which causes a more significant enhancement of neutral density around the cusp region under a resolution of 5° × 5°.

Simulations of meridional wind under the resolution of 5° × 5° (Figure 6a) and 5° × 1° (Figure 6b) along the HIWIND trajectory are compared with the observation. Under the resolution of 5° × 5°, the simulation with Cusp 2 (red-dashed line) is identical to that without additional cusp energy, but with Cusp 1, the meridional wind on the dayside turns equatorward. Under the resolution of 5° × 1°, persistent equatorward meridional wind is simulated on the dayside with both Cusp 1 and Cusp 2.

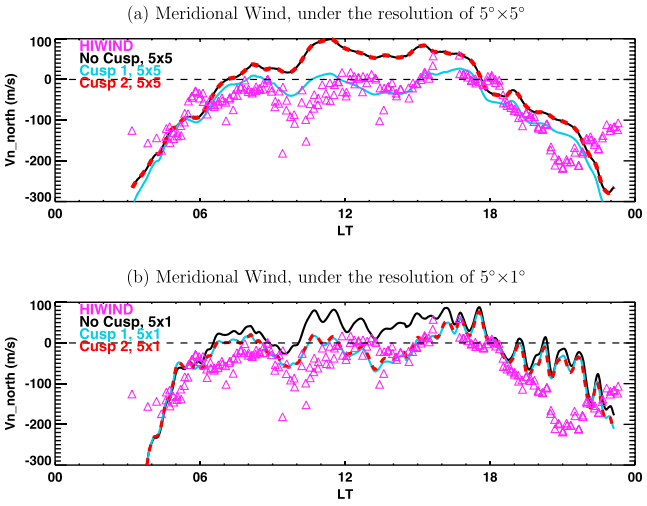

Figure 6. Comparisons of meridional wind between simulations and observation along the trajectory of HIWIND on 14 June 2011. The magenta triangle is for HIWIND observation, the black line is for the simulation without additional cusp energy, the blue line is for the simulation with Cusp 1, and the red-dashed line is for the simulation with Cusp 2. (a) Comparison under the resolution of 5° × 5°. (b) Comparison under the resolution of 5° × 1°.

Since accurate information on the cusp location and energy is difficult to obtain from observations, a fixed location and energy have been used for the cusp in this study, which is most likely quite different from the real case since the IMF B_Z varied between −5 and 10 nT during this time period. This approximation is used here since it may be sufficient for a mechanism study, to qualitatively show the influence of adding cusp energy on the horizontal neutral winds. Actually, the location of the cusp during the simulation period of 0000–2400 UT on 14 June 2011, from the predictions of the Lyon-Fedder-Mobarry global magnetosphere simulation [*Zhang et al.*, 2013], is very close to our specification. The deduced Poynting flux and soft electron precipitation from DMSP data are also consistent with our energy inputs (see supporting information Figure S1). Future studies will use the cusp specifications from an MHD model and the DMSP observations, which should allow a more quantitative comparison between the data and model.

4. Summary

The Global Ionosphere Thermosphere Model (GITM) is used to simulate the horizontal wind near the cusp region on 14 June 2011 driven by empirical high-latitude electrodynamic models, and the results have been compared with daytime HIWIND thermospheric wind observation. Without additional cusp energy, the simulation under the resolution of 5° × 1° shows poleward meridional wind on the equatorward side of the cusp. After including the additional cusp energy (Poynting flux and soft electron precipitation), the wind turns equatorward, which is consistent with the observations. The simulations reproduce the observed equatorward meridional wind on the dayside and suggest that the cusp energy has a strong impact on the neutral dynamics in and around the cusp region. The zonal component is not as well simulated with the additional cusp energy, which implies that the convection pattern or the longitudinal extent of the cusp may not have been specified precisely. Simulations using different resolutions (5° × 5° versus 5° × 1°) are compared as well. The results show that a resolution of 5° × 1° can resolve the cusp region consistently, while the simulations with a resolution of 5° × 5° can miss the cusp when it falls between grid points, which demonstrates the importance of simulation resolution.

Acknowledgments

This research at the University of Texas at Arlington was supported by NSF through grant ATM0955629, NASA through grants NNX13AD64G and NNX14AD46G, and AFOSR through award 1210429. The HIWIND project was supported by NASA grant NNX08AV35G. Q. Wu is also supported by NSF grant AGS1339918 and NASA grants NNX13AF93G and NNX14AD84G. NCAR is supported by the National Science Foundation. Please contact Cheng Sheng (cheng.sheng@mavs.uta.edu) for the model outputs used in this study. Please contact Q. Wu (qwu@ucar.edu) for HIWIND observations used in this paper. Please contact Ingemar Häggström for EISCAT observations used in this paper. EISCAT is an international association supported by research organizations in China (CRIRP), Finland (SA), Japan (NIPR and STEL), Norway (NFR), Sweden (VR), and the United Kingdom (NERC). We thank NASA Goddard Space Flight Center (http://omniweb.gsfc.nasa.gov/) for providing $F_{10.7}$ and SW/IMF data. We also thank NOAA Space Science Prediction Center (http://www.swpc.noaa.gov/) for providing the hemispheric power index data.

Alan Rodger thanks the reviewers for their assistance in evaluating this paper.

References

Deng, Y., and A. J. Ridley (2006), Dependence of neutral winds on convection E-field, solar EUV, and auroral particle precipitation at high latitudes, *J. Geophys. Res.*, *111*, A09306, doi:10.1029/2005JA011368.

Deng, Y., T. J. Fuller-Rowell, A. J. Ridley, D. Knipp, and R. E. Lopez (2013), Theoretical study: Influence of different energy sources on the cusp neutral density enhancement, *J. Geophys. Res. Space Physics*, *118*, 2340–2349, doi:10.1002/jgra.50197.

Eather, R. H. (1985), Polar cusp dynamics, *J. Geophys. Res.*, *90*, 1569–1576, doi:10.1029/JA090iA02p01569.

Fang, X., C. E. Randall, D. Lummerzheim, S. C. Solomon, M. J. Mills, D. R. Marsh, C. H. Jackman, W. Wang, and G. Lu (2008), Electron impact ionization: A new parameterization for 100 eV to 1 MeV electrons, *J. Geophys. Res.*, *113*, A09311, doi:10.1029/2008JA013384.

Frey, H. U. (2007), Localized aurora beyond the auroral oval, *Rev. Geophys.*, *45*, RG1003, doi:10.1029/2005RG000174.

Fuller-Rowell, T. J., and D.-S. Evans (1987), Height-integrated Pedersen and Hall conductivity patterns inferred from the TIROS-NOAA satellite data, *J. Geophys. Res.*, *92*, 7606–7618, doi:10.1029/JA092iA07p07606.

Kelley, M. C., D. J. Knudsen, and J. F. Vickrey (1991), Poynting flux measurements on a satellite: A diagnostic tool for space research, *J. Geophys. Res.*, *96*, 201–207, doi:10.1029/90JA01837.

Killeen, T. L., and R. G. Roble (1988), Thermosphere dynamics: Contributions from the first 5 years of the Dynamics Explorer Program, *Rev. Geophys.*, *26*, 329–367, doi:10.1029/RG026i002p00329.

Killeen, T. L., Y.-I. Won, R. J. Niciejewski, and A. G. Burns (1995), Upper thermosphere winds and temperatures in the geomagnetic polar cap: Solar cycle, geomagnetic activity, and interplanetary magnetic field dependencies, *J. Geophys. Res.*, *100*, 21,327–21,342, doi:10.1029/95JA01208.

Knipp, D., S. Eriksson, L. Kilcommons, G. Crowley, J. Lei, M. Hairston, and K. Drake (2011), Extreme Poynting flux in the dayside thermosphere: Examples and statistics, *Geophys. Res. Lett.*, *38*, L16102, doi:10.1029/2011GL048302.

Lühr, H., M. Rother, W. Köhler, P. Ritter, and L. Grunwaldt (2004), Thermospheric up-welling in the cusp region: Evidence from CHAMP observations, *Geophys. Res. Lett.*, *31*, L06805, doi:10.1029/2003GL019314.

Meriwether, J. W. (2006), Studies of thermospheric dynamics with a Fabry–Perot interferometer network: A review, *J. Atmos. Sol. Terr. Phys.*, *68*, 1576–1589, doi:10.1016/j.jastp.2005.11.014.

Newell, P. T., and C.-I. Meng (1987), Cusp width and B(z): Observations and a conceptual model, *J. Geophys. Res.*, *92*, 13,673–13,678, doi:10.1029/JA092iA12p13673.

Newell, P. T., and C.-I. Meng (1992), Mapping the dayside ionosphere to the magnetosphere according to particle precipitation characteristics, *Geophys. Res. Lett.*, *19*, 609–612, doi:10.1029/92GL00404.

Newell, P. T., C.-I. Meng, D. G. Sibeck, and R. Lepping (1989), Some low-altitude cusp dependencies on the interplanetary magnetic field, *J. Geophys. Res.*, *94*, 8921–8927, doi:10.1029/JA094iA07p08921.

Rees, D., P. J. Charleton, N. Lloyd, R. W. Smith, F. G. McCormac, and A. Steen (1984), The generation of vertical thermospheric winds and gravity waves at auroral latitudes—I. Observations of vertical winds, *Planet. Space Sci.*, *32*, 667–684, doi:10.1016/0032-0633(84)90092-8.

Rentz, S., and H. Lühr (2008), Climatology of the cusp-related thermospheric mass density anomaly, as derived from CHAMP observations, *Ann. Geophys.*, *26*, 2807–2823, doi:10.5194/angeo-26-2807-2008.

Richmond, A. D. (2010), On the ionospheric application of Poynting's theorem, *J. Geophys. Res.*, *115*, A10311, doi:10.1029/2010JA015768.

Ridley, A. J., Y. Deng, and G. Tóth (2006), The global ionosphere thermosphere model, *J. Atmos. Sol. Terr. Phys.*, *68*, 839–864, doi:10.1016/j.jastp.2006.01.008.

Rishbeth, H. (1972), Thermospheric winds and the F-region: A review, *J. Atmos. Terr. Phys.*, *34*, 1–47.

Smith, M. F., and M. Lockwood (1996), Earth's magnetospheric cusps, *Rev. Geophys.*, *34*, 233–260, doi:10.1029/96RG00893.

Thayer, J. P., G. Crowley, R. J. Niciejewski, T. L. Killeen, J. Buchau, and B. W. Reinisch (1995), Ground-based observations of ion/neutral coupling at Thule and Qanaq, Greenland, *J. Geophys. Res.*, *100*, 12,189–12,199, doi:10.1029/95JA00131.

Titheridge, J. E. (1995), Winds in the ionosphere—A review, *J. Atmos. Terr. Phys.*, *57*, 1681–1714.

Vontrat-Reberac, A., D. Fontaine, P.-L. Blelly, and M. Galand (2001), Theoretical predictions of the effect of cusp and dayside precipitation on the polar ionosphere, *J. Geophys. Res.*, *106*, 28,857–28,866, doi:10.1029/2001JA900131.

Weimer, D. R. (1996), A flexible, IMF dependent model of high-latitude electric potentials having "Space Weather" applications, *Geophys. Res. Lett.*, *23*, 2549–2552, doi:10.1029/96GL02255.

Wu, Q., W. Wang, R. G. Roble, I. Häggström, and A. Strømme (2012), First daytime thermospheric wind observation from a balloon-borne Fabry-Perot interferometer over Kiruna (68N), *Geophys. Res. Lett.*, *39*, L14104, doi:10.1029/2012GL052533.

Yordanova, E., D. Sundkvist, S. C. Buchert, M. André, Y. Ogawa, M. Morooka, O. Margithu, O. Amm, A. N. Fazakerley, and H. Réme (2007), Energy input from the exterior cusp into the ionosphere: Correlated ground-based and satellite observations, *Geophys. Res. Lett.*, *34*, L04102, doi:10.1029/2006GL028617.

Zhang, B., O. Brambles, W. Lotko, W. Dunlap-Shohl, R. Smith, M. Wiltberger, and J. Lyon (2013), Predicting the location of polar cusp in the Lyon-Fedder-Mobarry global magnetosphere simulation, *J. Geophys. Res. Space Physics*, *118*, 6327–6337, doi:10.1002/jgra.50565.

Zhou, X. W., C. T. Russell, G. Le, S. A. Fuselier, and J. D. Scudder (2000), Solar wind control of the polar cusp at high altitude, *J. Geophys. Res.*, *105*, 245–252, doi:10.1029/1999JA900412.